Impact of Wind Gusts on Detectability of GPS Spoofing Attacks Using RAIM with INS Coupling

Çağatay Tanıl, Samer Khanafseh, Boris Pervan
Illinois Institute of Technology

BIOGRAPHY

Çağatay Tanıl obtained his B.S. and M.S. in Mechanical Engineering from Middle East Technical University (METU), Turkey, in 2006 and 2009. He is currently a Ph.D. Candidate in Aerospace Engineering at Illinois Institute of Technology (IIT) and Research Assistant in Navigation and Guidance Lab. Prior to doctorate studies at IIT, he worked as a senior design engineer at several defense/aerospace companies (Roketsan Missiles Industries, TAI Turkish Aerospace Industries, Tubitak-SAGE Defense Industries Research and Development Institute) in Turkey from 2006 to 2013. He has been involved in flight mechanics, guidance, navigation and control, optimization, modeling and simulation, and path planning for autonomous systems in aerospace applications. He is currently focused on anti-spoofing attack algorithms for aircrafts.

Dr. Khanafseh is currently a Research Assistant Professor at Mechanical and Aerospace Engineering Department at IIT. He received his M.S. and PhD degrees in Aerospace Engineering from IIT, in 2003 and 2008, respectively. Dr. Khanafseh has been involved in several aviation applications such as Autonomous Airborne Refueling (AAR) of unmanned air vehicles, autonomous shipboard landing for NUCAS and JPALS programs and Ground Based Augmentation System (GBAS). He published 13 journal articles and more than 30 conference papers. His research interests are focused on high accuracy and high integrity navigation algorithms for close proximity applications, cycle ambiguity resolution, high integrity applications, fault monitoring and robust estimation techniques. He was the recipient of the 2011 Institute of Navigation Early Achievement Award for his outstanding contributions to the integrity of carrier phase navigation systems

Dr. Boris Pervan is a Professor of Mechanical and Aerospace Engineering at IIT, where he conducts research on advanced navigation systems. Prior to joining the faculty at IIT, he was a spacecraft mission analyst at Hughes Aircraft Company (now Boeing) and a postdoctoral research associate at Stanford University. Prof. Pervan received his B.S. from the University of Notre Dame, M.S. from the California Institute of Technology, and Ph.D. from Stanford University. He was the recipient of the IIT Sigma Xi Excellence in University Research Award, Ralph Barnett Mechanical and Aerospace Dept. Outstanding Teaching Award, Mechanical and Aerospace Dept. Excellence in Research Award, IIT University Excellence in Teaching Award, IEEE Aerospace and Electronic Systems Society M. Barry Carlton Award, RTCA William E. Jackson Award, Guggenheim Fellowship (Caltech), and the Albert J. Zahm Prize in Aeronautics (Notre Dame). He is an Associate Fellow of the AIAA, a Fellow of the Institute of Navigation (ION), and Editor-in-Chief of the ION Journal Navigation.

ABSTRACT

Vulnerability of GNSS users to signal spoofing is a critical threat to positioning integrity, especially in aviation applications where the consequences are potentially catastrophic. Spoofing may even become a more serious risk to aviation in the near future with the rollout of the GPS-based Next Generation Air Traffic Control (ATC) system, and the corresponding reduction in reliance on ground-based radar systems by ATC. In this work, we generalize the spoofing integrity analysis by deriving the statistical dynamic response of an aircraft to a vertical wind gust power spectrum (the Dryden Gust Turbulence model). In aircraft with INS-RAIM, the vehicle dynamic response to wind gusts provides an advantage for detection of the spoofing attack. The reason is that the aircraft response to a gust will be instantaneously reflected in INS measurements, but not in the spoofed GPS signal. The main contribution of this work is the development of a rigorous methodology to compute upper bounds on the integrity risk resulting from a worst case spoofing attack without needing to simulate individual aircraft approaches with an unmanageably large number specific gust disturbance profiles. We use a Boeing 747 aircraft model to demonstrate the performance of the INS-RAIM monitor under worst-case GPS spoofing and to investigate gust intensity levels that are sufficient to meet integrity risk requirements for precision landing approach.

I. INTRODUCTION

Civilian GNSS users are vulnerable to jamming and spoofing attacks. The main aim of such attacks is either to prevent positioning as in jamming or to feed the receiver false information so that it computes faulty positions as in spoofing. Unlike jamming which causes loss of signal, spoofing is a concealed attack which is a critical threat in aviation applications, where the possible catastrophic consequences justifies the need of

detecting this kind of deliberate interference [7]. In this work, we design, analyze and evaluate a new approach to directly detect spoofing using integrated Inertial Navigation Systems (INS) and fault detection concepts based on Receiver Autonomous Integrity Monitoring (RAIM). We describe a new method of quantifying the monitors integrity risk by leveraging an aircrafts response to wind gust disturbances, which is modeled using wind gust power spectral density function.

A spoofing attack happens when a counterfeit signal is deliberately broadcast to a target user, resulting in incorrect position estimates. The spoofed signal mimics the original GPS signal with higher power and thus may go unnoticed by measurement screening techniques used within the receiver. As a result, the trajectory of the target user can be controlled through the fake broadcast measurements [1]. Numerous anti-spoofing techniques have been developed, including employing modified GPS navigation data [2], using antenna arrays and automatic gain control schemes [3], high-frequency antenna motion [4], or signal power analysis techniques. Intuitive approaches to monitor for spoof attacks using redundant sensors have also been proposed, however the first thorough description of their implementation and performance in terms of probability of false alarm and probability of missed detection was first introduced in [6].

The detector we proposed in [6] monitors discrepancies between GPS spoofed measurements and INS measurements. For that monitor, the INS unit is assumed to be pre-calibrated under nominal error conditions prior to a spoofing attack. For the tightly coupled implementation, continuous calibration of INS errors increases monitor sensitivity to position-domain discrepancies caused by the spoofing attack. This feature was exploited together with a time history of residuals in designing an efficient detection algorithm for GPS spoofing using residual based RAIM.

RAIM detection concepts were used where the redundancy is provided through INS measurements, unlike conventional usage of RAIM where detection is provided through satellite redundancy. To enhance detection capability, a time history of GPS measurements is used to estimate the position vector and compute measurement residuals in a batch weighted least squares estimator. When using residual-based RAIM, it is not necessary to define a threat space because the worst-case sequence of spoofed GPS measurements can be determined analytically by finding the profile that maximizes integrity risk [5]. This profile takes into account the impact of spoofed signals on the test statistic and on user position estimate errors.

In previous work, we illustrated how a spoofer can inject faults slowly into the GPS measurements such that they corrupt the tightly coupled solution while going unnoticed by the RAIM detector [6]. It was also shown that if the spoofer knows the exact trajectory of an aircraft, he or she might eventually cause errors large enough to exceed hazard safety limits, again without triggering an alarm from the RAIM detector. However, it was acknowledged that in reality, actual trajectory of the aircraft would always deviate somewhat from a prescribed path (e.g., a straight line final approach) due to natural disturbances such as wind gusts. Deviations from the nominal trajectory due to gust disturbances, which are initially assumed to be unknown to the spoofer, would enhance detection capability of the INS RAIM monitor.

As a case study in [6], in the presence of simple sinusoidal deviations from a nominal straight trajectory, it was concluded that the monitor was effective, for the cases tested at least, in detecting spoofing attacks with quantifiably low integrity risk. However, to make a decisive conclusion, the aircraft trajectory must be tested with generalized disturbance patterns.

In this work, we extend the spoofing integrity analysis by deriving the statistical dynamic response of an aircraft to a well-established wind gust power spectrum (the Dryden Gust Turbulence model). This derivation provides a statistical quantification of the trajectory deviations for a stochastic gust environment. This information was incorporated to the monitor by deriving a new formulation of the GPS/INS RAIM monitor. Typically, INS measurements are used as inputs or to populate the dynamic propagation matrix. In this new batch formulation, INS measurements appear as a part of the measurement vector instead. As a result, the impact of the disturbance on the aircraft nominal trajectory can be directly incorporated in the fault vector in a seamless fashion. Then, a worst-case fault profile that maximizes integrity risk is computed. After evaluating the performance of this new monitor for an example aircraft landing approach under exposure to a stochastic wind gust environment, it is shown that the new monitor meets the integrity risk requirement for aircraft precision approaches.

II. GPS-INS AIRBORNE RAIM MONITOR

RAIM was originally developed to detect satellite faults by exploiting the extra redundancy in satellite measurements. The residual vector is defined as the difference between the predicted measurements and the actual measurements. In residual based RAIM the test statistic is defined as the weighted norm of the residual vector. Under fault free conditions, the statistical behavior of the test statistic is governed by the measurement noise characteristics. For a given false alarm requirement, these characteristics are used to define a threshold for the RAIM monitor. Unlike conventional RAIM usage, RAIM detection concepts used in this work provides the redundancy through INS measurements.

GPS and inertial navigation systems can be coupled using a variety of integration schemes. These can range from the simple loosely coupled integration, to the complex ultra-tightly coupled mode in which the INS directly aids the GPS tracking loops [6]. This work uses tightly-coupled integration since the worst-case fault vector in [6] is derived for tightly-coupled formulation.

it enhances fault detection capability of the aircraft by exploiting the impact of faulty GPS measurements on INS error state estimates through a tightly-coupled mechanism.

Within the various disturbances on the aircraft motion, wind gust has a significant impact that improves monitor sensitivity to position-domain discrepancies due to spoofing attack. The previous study in [6] proved that if the spoofer have the exact

position information of the aircraft, it is impossible to detect a spoofing with the worst-case fault. On the other hand, in INS-RAIM-equipped aircrafts, the vehicle dynamic response to wind gust provides a direct means for detection of the spoofing attack. The reason is that the aircraft response to gust will be instantaneously reflected in INS measurements, but not in the spoofed GPS signal. This increases position discrepancy between INS and GPS in the batch form.

A. Actual monitor

Before investigating the impact of wind gust on the detection capability of the RAIM monitor, we should define the actual RAIM monitor with INS-GPS integration which will be implemented on aircrafts.

Linearized process model obtained from INS mechanization contains both aircraft kinematics and IMU bias model and can be expressed in vector form as

$$\boldsymbol{x} = \boldsymbol{F}\boldsymbol{x} + \boldsymbol{G}_w\boldsymbol{w} \tag{1}$$

where $\boldsymbol{x} = [\delta\boldsymbol{r}, \delta\boldsymbol{v}, \delta\boldsymbol{E}, \boldsymbol{b}]^T$ is the augmented INS state vector including errors in position $\boldsymbol{r}$, velocity $\boldsymbol{v}$, attitude $\boldsymbol{E}$ and bias state vector $\boldsymbol{b}$ including gyroscope and accelerometer biases. Note that these are linearized about actual trajectory values. The second term in right hand side of (1) stands for the noise due to IMU sensors where $\boldsymbol{w}$ is the noise vector containing white and bias driving noises: $\boldsymbol{\nu}_n$ and $\boldsymbol{\eta}_b$ respectively, and $\boldsymbol{G}_w$ is the noise coefficient matrix. More details about the derivation of INS mechanization will be introduced in Section IV and Appendix C.

The double-difference (DD) carrier and code GPS measurement equation is given as a function of state vector of the actual system $\boldsymbol{x}$ as

$$\boldsymbol{z} = \boldsymbol{G}\boldsymbol{x} + \boldsymbol{D}\boldsymbol{N} + \boldsymbol{\nu}_{\rho\phi} + \boldsymbol{f} \tag{2}$$

where $\boldsymbol{z}$ includes carrier and code measurements after correcting with the nominal terms. The first three columns of $\boldsymbol{G}$ associated with $\delta\boldsymbol{r}$ is line-of-sight vectors, the rest of the columns associated with the rest of the elements in $\boldsymbol{x}$ is all zeros, $\boldsymbol{N}$ and $\boldsymbol{D}$ are the cycle ambiguity state vector and its constant coefficient matrix respectively, $\boldsymbol{\nu}_{\rho\phi}$ is the DD carrier and code measurement error vector and $\boldsymbol{f}$ denotes fault vector due to spoofing attack. More details about measurement model is given in Section V-A and Appendix D.

After discretizing the equations in (1) and (2), their time history can be stacked in a batch form as it will be explained in Section V-A and it yields one single batch equation in the form of

$$\boldsymbol{z}_b = \boldsymbol{H}_b\,\boldsymbol{x}_b + \boldsymbol{\nu}_b + \boldsymbol{f}_b \tag{3}$$

where $\boldsymbol{x}_b = [\boldsymbol{x}_1, \boldsymbol{x}_2, ...]^T$, $\boldsymbol{z}_b = [\boldsymbol{z}_1, \boldsymbol{z}_2, ...]^T$ and, $\boldsymbol{H}_b$ is the overall observation matrix of the actual system containing the INS and GPS information. Similarly, $\boldsymbol{\nu}_b$ is the noise vector including both GPS and process noise. Note that the subscript b is used to refer to the batch form.

The residual vector of the actual system $\boldsymbol{r}$ is defined as

$$\boldsymbol{r} = \boldsymbol{z}_b - \boldsymbol{H}_b\,\hat{\boldsymbol{x}}_b \tag{4}$$

and can be simplified to

$$\boldsymbol{r} = \big(\boldsymbol{I} - \boldsymbol{H}_b\,\boldsymbol{S}_b\big)\big(\boldsymbol{v}_b + \boldsymbol{f}_b\big) \tag{5}$$

where $\boldsymbol{S}_b$ is the pseudo-inverse matrix for the actual batch system and is computed as

$$\boldsymbol{S}_b = \hat{\boldsymbol{P}}_b\,\boldsymbol{H}_b^T\,\boldsymbol{V}_b^{-1} \tag{6}$$

where $\hat{\boldsymbol{P}}_b$ is the state estimate covariance matrix

$$\hat{\boldsymbol{P}}_b = \big(\boldsymbol{H}_b^T\,\boldsymbol{V}_b^{-1}\boldsymbol{H}_b\big)^{-1} \tag{7}$$

RAIM monitor of the actual system checks whether weighted norm of the residual, which is called test statistics q, is smaller than a pre-defined threshold T^2 as below

$$q = \boldsymbol{r}^T\boldsymbol{V}_b^{-1}\boldsymbol{r} < T^2 \tag{8}$$

Let n be the number of measurements, and m be the number of states. Under fault free conditions, the test statistic q is centrally chi-square distributed with $(n-m)$ degrees of freedom. For a given false alarm requirement, the threshold T is determined from the inverse cumulative chi-square distribution. RAIM alarms for a fault if q is bigger than T^2.

B. Monitor Performance Evaluation

A wide variety of possible spoofing scenarios may exist, but when using residual-based RAIM, it is not necessary to define a threat space because the worst-case spoofing attack can be determined by finding the profile that maximizes the integrity risk [5]. This profile takes into account the impact of spoofed signals on the test statistic and the user position estimate error simultaneously.

State estimation error $\boldsymbol{\varepsilon} = \hat{\boldsymbol{x}}_b - \boldsymbol{x}_b$ can be computed as

$$\boldsymbol{\varepsilon} = \boldsymbol{S}_b\,\big(\boldsymbol{\nu}_b + \boldsymbol{f}_b\big) \tag{9}$$

Since the error in altitude is the most critical in landing approach and vertical requirements are usually the most stringent, it is convenient to evaluate the performance with respect to vertical direction only [6]. The error associated with the altitude is related to $\boldsymbol{\varepsilon}$ as

$$\varepsilon = \boldsymbol{s}_b^T\,\big(\boldsymbol{\nu}_b + \boldsymbol{f}_b\big) \tag{10}$$

where $\boldsymbol{s}_b^T$ is a single row of the matrix $\boldsymbol{S}_b$ corresponding to altitude.

In this work, since all GPS measurements may be impacted by the spoofing attack, it is assumed that all GPS measurements are faulty and that INS is the source of redundancy in RAIM. If a spoofing attack is not detected instantaneously, it may impact INS error state estimates through the tightly coupled mechanism, which impacts subsequent detection capability. Therefore, a smart spoofer may select a fault profile that has smaller faults at the beginning, but increases over time. The worst case fault profile is one that is injected slowly into the GPS measurements, thereby corrupting INS calibration without being detected.

Finding the worst case fault profile for least squares RAIM has been derived in [21] and was extended to batch estimation

in [5]. Under faulted conditions, q is non-centrally chi-square distributed with $(n-m)$ degrees of freedom and a non-centrality parameter λ^2

$$\lambda^2 = \boldsymbol{f}_b^T \boldsymbol{V}_b^{-1} \big(\boldsymbol{I} - \boldsymbol{H}_b \boldsymbol{S}_b\big) \boldsymbol{f}_b \tag{11}$$

Integrity risk is a metric to evaluate the performance of the RAIM monitor and is defined as the probability that the position error ε exceeds an alert limit l without being detected (i.e. $q < T^2$). It has been shown in [16] that ε and q are statistically independent. Therefore, integrity risk I_r can be written as a multiplication of two probabilities as

$$I_r = P\{|\varepsilon| > l\}\, P\{q < T^2\} \tag{12}$$

The worst case fault vector that maximizes the integrity risk was derived in [5] as

$$\boldsymbol{f}_{w_b} = \alpha \boldsymbol{A} \boldsymbol{M}_A \boldsymbol{M}_A^T \boldsymbol{M}_X^T \tag{13}$$

where $\boldsymbol{M}_A$, $\boldsymbol{M}_X$ and $\boldsymbol{A}$ are defined and analytically optimized in [5] as a function of $\boldsymbol{H}_b$ and $\boldsymbol{V}_b$. α is a scalar that is determined through iteration to maximize I_r. The fault vector in (13) represents the most dangerous fault profile that a spoofer can inject into the GPS measurements and represents the most dangerous threat for aviation users.

As discussed in the introduction, wind gust may assist the detection of spoofing faults because the actual (resultant) fault will be different than the worst-case fault that the spoofer injects to the system. To evaluate RAIM performance, we will first introduce the wind gust and aircraft dynamic models to obtain the aircraft response to wind gust, and the tightly-coupled INS/GPS integration.

III. WIND GUST AUGMENTED AIRCRAFT FLIGHT DYNAMIC MODEL

The atmosphere is composed of many individual patches of continuous turbulence, each of which may be described by a power spectral density. To model atmospheric turbulence, a random velocity disturbance is generated by filtering a white noise, the variance of which is assumed to be root-mean-square (rms) gust velocity intensity [17]. Utilizing this stochastic model for longitudinal gust dynamics provides a generalized statistical approach to evaluate gust impacts on aircraft instead of running numerous deterministic gust profiles in Monte-Carlo flight simulations.

In Fig. 1, a block diagram for generating the vertical spatial components of gust velocity is given. Driving the second-order linear and first-order angular filters G_{w_g} and G_{q_g} with a white noise η_g yields linear vertical gust velocity and angular pitch rate q which can be used as wind disturbance inputs for an aircraft dynamic system. Within a variety of existing gust filter models, the Dryden and Von Karman models are generally used for continuous gusts in flight dynamics applications. In this work, we chose the Dryden Model to represent longitudinal (vertical) gust dynamics, which is expressed in state-space form (details are in Appendix A) as

$$\dot{\boldsymbol{x}}_g = \boldsymbol{A}_g \boldsymbol{x}_g + \boldsymbol{b}_g \eta_g \tag{14}$$

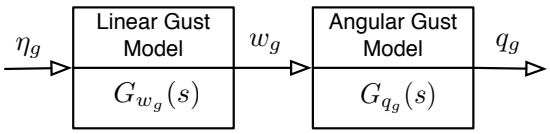

Fig. 1. The Dryden Vertical Wind Turbulence Model

where $\eta_g \sim \mathcal{N}(0, \sigma_g^2)$, and the first two elements in $\boldsymbol{x}_g$ are vertical gust states, and the last element is related to pitch rate. The disturbances to wind vertical velocity and longitudinal angular velocity can be output as a function of gust states as

$$\boldsymbol{w}_g = \boldsymbol{c}_g^T \boldsymbol{x}_g \tag{15}$$

where $\boldsymbol{w}_g = [w_g, q_g]^T$ and $\boldsymbol{c}_g^T$ is constant row vector defined in Appendix A.

Flight through choppy air easily excites the short period oscillations for the aircraft. Therefore, for an airplane in level flight the main source of excitation is the turbulence disturbance [8]. These disturbances are not anticipated by the spoofer, but sensed by the IMU, which provides the means to detect spoofing attacks. The output of the wind gust model $\boldsymbol{w}_g$ can then be treated as a disturbance to the linearized vertical aircraft dynamics which can be described as

$$\delta \dot{\boldsymbol{x}}_d = \boldsymbol{F}_d\, \delta \boldsymbol{x}_d + \boldsymbol{G}_g \boldsymbol{w}_g \tag{16}$$

where $\delta \boldsymbol{x}_d = [u, w, q, \theta]^T$ including vertical plane velocity components (u, w), and pitch rate q, and angle θ. $\boldsymbol{G}_g$ is the wind gust disturbance coefficient matrix, the columns of which are the same as the second and third columns of aircraft plant matrix $\boldsymbol{F}_d$ defined in Appendix B.

Since the gust noise vector $\boldsymbol{w}_g$ in (16) is driven by the gust dynamic model defined in (14) and (15), gust-augmented aircraft dynamic model in state-space form can be written as

$$\left[\begin{array}{c} \delta \dot{\boldsymbol{x}}_d \\ \hline \dot{\boldsymbol{x}}_g \end{array}\right] = \underbrace{\left[\begin{array}{c|c} \boldsymbol{F}_d & \boldsymbol{G}_g\, \boldsymbol{c}_g^T \\ \hline 0 & \boldsymbol{A}_g \end{array}\right]}_{\boldsymbol{F}_{dg}} \underbrace{\left[\begin{array}{c} \delta \boldsymbol{x}_d \\ \hline \boldsymbol{x}_g \end{array}\right]}_{\boldsymbol{x}_{dg}} + \underbrace{\left[\begin{array}{c} \boldsymbol{0} \\ \hline \boldsymbol{b}_g \end{array}\right]}_{\boldsymbol{G}_g'} \eta_g \tag{17}$$

where $\boldsymbol{G}_g'$ is the noise coefficient matrix of the augmented dynamic model, $\boldsymbol{F}_{dg}$ is the augmented plant matrix, and $\boldsymbol{x}_{dg}$ is the augmented dynamic state vector capturing the additional gust states.

Since we perform a power spectral analysis, our main goal is to obtain the covariance on position deviation $\delta \boldsymbol{r}_w$ due to wind gust. To achieve this, we first need to compute the covariance on augmented aircraft dynamic states $\boldsymbol{x}_{dg}$ and integrate it over time to obtain the covariance on position deviation. Assuming

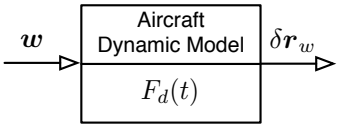

Fig. 2. Aircraft Flight Dynamic Model

steady-state wind gust conditions and knowing that the gust filters $\boldsymbol{G}_{w_g}$ and $\boldsymbol{G}_{q_g}$, and aircraft model $\boldsymbol{F}_d$ are stable, we can obtain the steady-state covariance of $\boldsymbol{x}_{dg}$ by numerically solving the Lyapunov equation obtained from augmented state equation in (17) as

$$0 = \boldsymbol{F}_{dg}\boldsymbol{X}^s_{dg} + \boldsymbol{X}^s_{dg}\boldsymbol{F}^T_{dg} + \boldsymbol{G}^{'}_{w}\boldsymbol{G}^{'^T}_{w}\eta_g \tag{18}$$

where $\boldsymbol{X}^s_{dg}$ is the steady-state covariance of augmented state $\boldsymbol{x}_{dg}$. The superscript s stands for steady-state values.

The output $\delta\boldsymbol{r}_w$ of the linearized aircraft model in Fig. 2, which will feed GPS measurement model in performance evaluation, contains the deviations in aircraft position due to wind gust. This represents the difference in position obtained from fake GPS measurements the spoofer broadcasts and the actual position obtained from propogated IMU measurements and can be expressed in terms of steady-state augmented aircraft state $\boldsymbol{x}^s_{dg}$ as

$$\delta\dot{\boldsymbol{r}}_w = \underbrace{\left[\begin{array}{c|c} \boldsymbol{J}_{dr} & 0 \end{array}\right]}_{\boldsymbol{J}_r} \left[\frac{\delta\boldsymbol{x}_d}{\boldsymbol{x}_g}\right]^s \tag{19}$$

where $\boldsymbol{J}_{dr}$ is a constant matrix composed of ones and zeros that transform longitudinal aircraft states $\boldsymbol{x}_d$ to the derivative of position deviations from nominal trajectory. Discrete form of (19) is

$$(\delta\boldsymbol{r}_w)_{k+1} = (\delta\boldsymbol{r}_w)_k + \boldsymbol{\Gamma}_{r_k}\boldsymbol{x}^s_{dg_k} \tag{20}$$

where $\boldsymbol{\Gamma}_{r_k}$ is the discrete form of $\boldsymbol{J}_r$.

We can propagate the position covariance over time as

$$(\boldsymbol{R}_w)_{k+1} = (\boldsymbol{R}_w)_k + \boldsymbol{\Gamma}_{r_k}\boldsymbol{X}^s_{dg_k}\boldsymbol{\Gamma}^T_{r_k} \tag{21}$$

where $\boldsymbol{R}_w$ is the covariance matrix for position deviations from nominal due to wind gust. $\delta\boldsymbol{r}_w \sim \mathcal{N}(0, \boldsymbol{R}_w)$ will be utilized when formulating the resultant fault vector in Section V-B.

Recall that we will utilize the gust and aircraft dynamic models to evaluate the detection performance of the monitor to GPS spoofed signals. In practice, the aircraft dynamic model will not be utilized in actual aircrafts navigation system.

IV. INS KINEMATIC MODEL

INS mechanization equations represent a kinematic model where the input the IMU measurements (inertial acceleration and angular velocity), and the output is the position, velocity and attitude in a frame of interest. In this case, the frame of interest is a local navigation frame (N). Since our motivation is detecting spoofing during aircraft landing approaches, we integrate INS with differential GPS (DGPS). For consistency and simplicity in the derivation of the mechanization equations, we define the frame of interest as being fixed at the reference station (r) having axes in east, north, and up (Fig. 3). Since the IMU outputs the inertial acceleration and angular velocity expressed in the aircraft body frame (B), we need a kinematic model that transforms vectors from B-frame to those in N-frame. In order to be consistent with the derivation of the augmented aircraft dynamic, we linearize the INS system

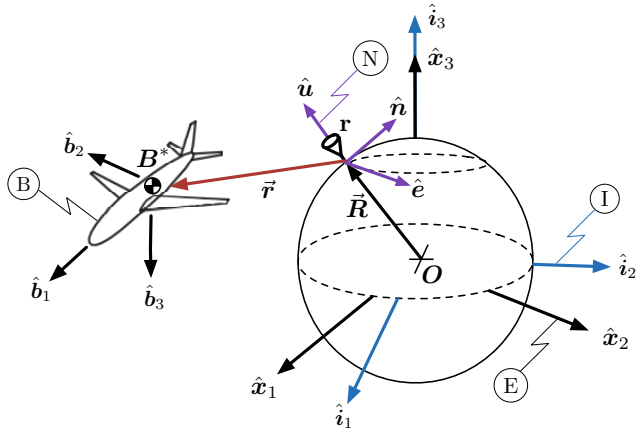

Fig. 3. Coordinate Frames

about nominal trajectory as illustrated in Fig. 4. Assuming the position deviations due to wind gust are small, the impact of these deviations on INS mechanization is considered a second order effect, which can be neglected.The INS kinematic model linearized about nominal values can be expressed in a vector form as

$$\delta\dot{\boldsymbol{x}}_n = \boldsymbol{F}_n\,\delta\boldsymbol{x}_n + \boldsymbol{G}_u\,\delta\boldsymbol{u} \tag{22}$$

where $\delta\boldsymbol{x}_n = [\delta\boldsymbol{r}, \delta\boldsymbol{v}, \delta\boldsymbol{E}]^T$ is referred to as the INS state vector including deviations in position $\boldsymbol{r}$, velocity $\boldsymbol{v}$, and attitude $\boldsymbol{E}$ of the aircraft. $\boldsymbol{F}_n$ is plant matrix of the kinematic model, $\boldsymbol{G}_u$ is input coefficient matrix, and $\delta\boldsymbol{u}$ is the IMU measurement errors of the specific force and angular velocity relative to inertial frame as

$$\delta\boldsymbol{u} = \begin{bmatrix} \delta\boldsymbol{f}^{(b)} \\ \delta\boldsymbol{\omega}^{(b)}_{ib} \end{bmatrix} \tag{23}$$

Measurement errors include accelerometer and gyroscope biases, captured in vector $\boldsymbol{b}$ and white noise vector $\boldsymbol{\nu}$ as

$$\delta\boldsymbol{u} = \boldsymbol{b} + \boldsymbol{\nu}_n \tag{24}$$

where $\boldsymbol{\nu}_n$ is a 6×1 vector including accelerometer and gyroscope white noises, which are uncorrelated and zero-mean and $\boldsymbol{b}$ is a 6×1 vector that is modeled as a first order Gauss Markov process as

$$\dot{\boldsymbol{b}} = \frac{1}{\boldsymbol{\tau}}\boldsymbol{b} + \boldsymbol{\eta}_b \tag{25}$$

where $\boldsymbol{\eta}_b$ represents the bias driving white noise and $\boldsymbol{\tau}$ represents the time constants of biases.

Augmenting bias dynamics in (25) with the INS error kinematic model in (22) yields an augmented dynamic model for INS system as

$$\begin{bmatrix} \delta\dot{\boldsymbol{x}}_n \\ \dot{\boldsymbol{b}} \end{bmatrix} = \underbrace{\begin{bmatrix} \boldsymbol{F}_n & \boldsymbol{G}_u \\ 0 & {}^1\!/\boldsymbol{\tau} \end{bmatrix}}_{\boldsymbol{F}} \underbrace{\begin{bmatrix} \delta\boldsymbol{x}_n \\ \boldsymbol{b} \end{bmatrix}}_{\boldsymbol{x}} + \underbrace{\begin{bmatrix} \boldsymbol{G}_u & 0 \\ 0 & \boldsymbol{I} \end{bmatrix}}_{\boldsymbol{G}_w} \underbrace{\begin{bmatrix} \boldsymbol{\nu}_n \\ \boldsymbol{\eta}_b \end{bmatrix}}_{\boldsymbol{w}} \tag{26}$$

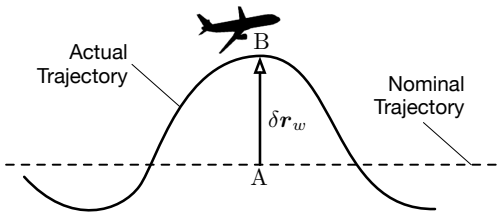

Fig. 4. Variations in Position due to Wind Gust Disturbance

V. RAIM PERFORMANCE EVALUATION MODEL

So far, we derived a dynamic model in (17) capturing the aircraft response to wind gust disturbance and a process model for INS system in (26). To perform a covariance analysis for performance evaluation of the actual RAIM under GPS spoofing attacks, GPS measurement model should be first integrated with the INS model derived in (26). Then, the actual RAIM implemented on aircrafts will be reformulated using this tightly-coupled INS/GPS mechanism and augmented aircraft dynamics derived in Section III.

A. Tightly-Coupled INS/GPS Integration

Since the main focus of this work is to detect spoofing during landing phase of the flight, measurement equations are constructed based on DD GPS. The GPS code and carrier phase measurement equation can be represented in linear form as

$$\boldsymbol{z} = \boldsymbol{G}^* \delta \boldsymbol{r}^{(n)} + \boldsymbol{D}\boldsymbol{N} + \boldsymbol{\nu}_{\rho\phi} + \boldsymbol{f}_r \tag{27}$$

where $\boldsymbol{z}$ is the measurement vector containing carrier and code phase measurements, $\boldsymbol{G}^*$ is the observation matrix including line-of-sight information from the reference station to the satellites in the navigation frame. $\delta \boldsymbol{r}^{(n)}$ is the variation on the position of the aircraft relative to reference station represented in navigation frame N. $\boldsymbol{N}$ and $\boldsymbol{D}$ are the cycle ambiguity state vector and its constant coefficient matrix, respectively and $\boldsymbol{\nu}_{\rho\phi}$ is the DD carrier and code measurement error vector. $\boldsymbol{f}_r$ denotes the resultant fault vector due to a spoofing attack.

By using GPS-aided INS navigation system, INS error drift is bounded, which allows INS to be used as a consistency check against GPS spoofing attacks. In tightly coupled mechanism, raw INS and GPS data are processed in a unified filter [13]. In order to be able to compute the worst-case fault using the algorithm developed for batch estimators in [5], we stack the process model in (26) and measurement model in (27) in a single batch and use a least-square estimator to compute the state estimate covariance. In the tightly coupled integration, coupling between process model and GPS measurement model can be obtained by first relating the state vector $\delta \boldsymbol{r}^{(n)}$ in GPS measurement model to the state vector $\boldsymbol{x}$ used in overall augmented dynamic model (26) as

$$\boldsymbol{z} = \underbrace{\left[\begin{array}{c|c} \boldsymbol{G}^* & \boldsymbol{0} \end{array}\right]}_{\boldsymbol{G}} \underbrace{\left[\begin{array}{c} \delta \boldsymbol{r}^{(n)} \\ \hline \vdots \end{array}\right]}_{\boldsymbol{x}} + \boldsymbol{D}\boldsymbol{N} + \boldsymbol{\nu}_{\rho\phi} + \boldsymbol{f}_r \tag{28}$$

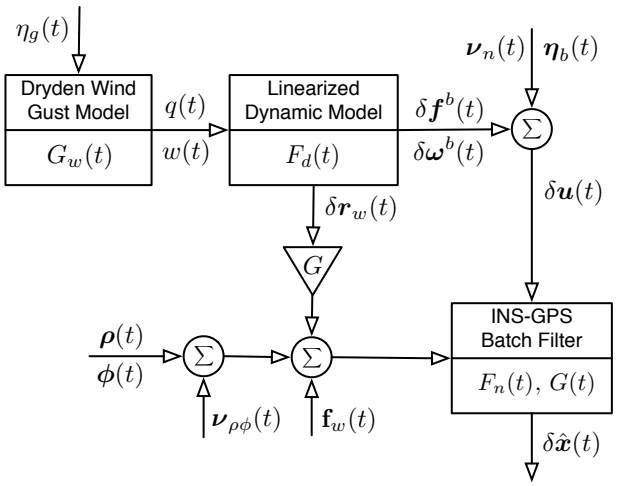

Fig. 5. Tightly Coupled INS-GPS Mechanism and its Interaction with Aircraft and Wind Gust Dynamics for RAIM Performance Evaluation

where dotted terms are the rest of the states in the augmented INS error state vector $\boldsymbol{x}$ except position $\delta \boldsymbol{r}^{(n)}$.

The continuous measurement model together with the augmented INS model can be written as

$$\boldsymbol{z} = \boldsymbol{G}\boldsymbol{x} + \boldsymbol{D}\boldsymbol{N} + \boldsymbol{\nu}_{\rho\phi} + \boldsymbol{f}_r \tag{29}$$

$$\dot{\boldsymbol{x}} = \boldsymbol{F}\boldsymbol{x} + \boldsymbol{G}_w \boldsymbol{w} \tag{30}$$

which can be expressed in a discrete form as

$$\boldsymbol{z}_k = \boldsymbol{G}_k \boldsymbol{x}_k + \boldsymbol{D}\boldsymbol{N} + \boldsymbol{\nu}_{\rho\phi_k} + \boldsymbol{f}_{r_k} \tag{31}$$

$$0 = \boldsymbol{\Phi}_k \boldsymbol{x}_k - \boldsymbol{I}\boldsymbol{x}_{k+1} + \boldsymbol{\Gamma}_{w_k} \boldsymbol{w}_k \tag{32}$$

where $\boldsymbol{\Phi}$ and $\boldsymbol{\Gamma}_w$ are the discrete state transition matrix and noise coefficient matrix of the augmented INS system. Note that the cycle ambiguity vector $\boldsymbol{N}$ is constant over time as long as there are no cycle slips during flight.

So far, we obtained a discrete measurement model in (31) and a process model in (32) in Kalman form. The next step is to construct a batch form of tightly-coupled INS/GPS mechanism by using (31) and (32). To increase the observability of the batch model, it is assumed that the INS and cycle ambiguity states have been initialized in a fault-free condition as

$$\underbrace{\left[\begin{array}{c} \boldsymbol{x}_0 \\ \boldsymbol{N}_0 \end{array}\right]}_{\boldsymbol{x}_0^N} = \underbrace{\left[\begin{array}{c} \boldsymbol{I} \\ 0 \end{array}\right]}_{\boldsymbol{I}_0} \boldsymbol{x}_1 + \underbrace{\left[\begin{array}{c} 0 \\ \boldsymbol{I} \end{array}\right]}_{\boldsymbol{D}_0} \boldsymbol{N} + \boldsymbol{w}_0 \tag{33}$$

where $\boldsymbol{w}_0 \sim \mathcal{N}(0, \boldsymbol{W}_0)$ and $\boldsymbol{W}_0$ is the initial covariance matrix. In this work, the initial covariance can be obtained from a Kalman Filter running during presumed fault free period.

Combining (31), (32) and (33) yields a batch form containing all the time history of process and measurement models

with initial conditions as

$$\overbrace{\begin{bmatrix} \boldsymbol{x}_0^N \\ \boldsymbol{z}_1 \\ 0 \\ \boldsymbol{z}_2 \\ 0 \\ \vdots \end{bmatrix}}^{\boldsymbol{z}_b} = \overbrace{\begin{bmatrix} \boldsymbol{I}_0 & & & \boldsymbol{D}_0 \\ \boldsymbol{G}_1 & & & \boldsymbol{D} \\ \boldsymbol{\Phi}_1 & -\boldsymbol{I} & 0 & 0 \\ & \boldsymbol{G}_2 & & \boldsymbol{D} \\ & \boldsymbol{\Phi}_2 & -\boldsymbol{I} & 0 \\ 0 & & \ddots & \vdots \end{bmatrix}}^{\boldsymbol{H}_b} \overbrace{\begin{bmatrix} \boldsymbol{x}_1 \\ \boldsymbol{x}_2 \\ \boldsymbol{x}_3 \\ \boldsymbol{x}_4 \\ \vdots \\ \boldsymbol{N} \end{bmatrix}}^{\boldsymbol{x}_b} + \underbrace{\begin{bmatrix} \boldsymbol{w}_0 \\ \boldsymbol{\nu}_{\rho\phi_1} \\ \boldsymbol{\Gamma}_{w_1}\boldsymbol{w}_1 \\ \boldsymbol{\nu}_{\rho\phi_2} \\ \boldsymbol{\Gamma}_{w_2}\boldsymbol{w}_2 \\ \vdots \end{bmatrix}}_{\boldsymbol{\nu}_b} + \underbrace{\begin{bmatrix} 0 \\ \boldsymbol{f}_{r_1} \\ 0 \\ \boldsymbol{f}_{r_2} \\ 0 \\ \vdots \end{bmatrix}}_{\boldsymbol{f}_{r_b}} \tag{34}$$

where $\boldsymbol{z}_b$ is the batch measurement vector, $\boldsymbol{H}_b$ is the batch observation matrix, $\boldsymbol{x}_b$ is the batch state vector, $\boldsymbol{f}_{r_b}$ is the resultant fault vector in a batch form, and $\boldsymbol{\nu}_b \sim \mathcal{N}(0, \boldsymbol{V}_b)$ is the batch measurement noise vector, which has a zero-mean with a covariance matrix $\boldsymbol{V}_b$ in (35).

$$\boldsymbol{V}_b = \begin{bmatrix} \boldsymbol{W}_0 & & 0 & & \\ & \boldsymbol{V}_{\rho\phi_1} & & \boldsymbol{V}_{\rho\phi_{12}} & \cdots \\ & & \boldsymbol{\Gamma}_{w_1}\boldsymbol{W}_1\boldsymbol{\Gamma}_{w_1}^T & & \\ & 0 & & \boldsymbol{V}_{\rho\phi_2} & \\ & & & & \ddots \end{bmatrix} \tag{35}$$

The first diagonal term in (35) corresponds to initial covariance matrix. Diagonal terms $\boldsymbol{V}_{\rho\phi_i}$ include thermal noise and multi-path, while the time correlated effect of multipath is captured in the off-diagonal terms $\boldsymbol{V}_{\rho\phi_{ij}}$ where multipath is modeled as a first order Gauss Markov process.

Since the initial condition is already included into the batch, state estimate covariance $\hat{\boldsymbol{P}}_b$ can be computed using a weighted least squares batch estimator as

$$\hat{\boldsymbol{P}}_b = \left(\boldsymbol{H}_b^T \, \boldsymbol{V}_b{}^{-1} \boldsymbol{H}_b\right)^{-1} \tag{36}$$

In Fig. 6, the blue line represents the spoofing trajectory, the black dotted line is the nominal or planned trajectory, the black curved trajectory is the actual flight path deviated from nominal trajectory due to wind gust, and the red line is the trajectory the aircraft will maneuver to after responding to the spoofed signal. For the covariance analysis we perform in this work, we assume that the aircraft guidance and control system

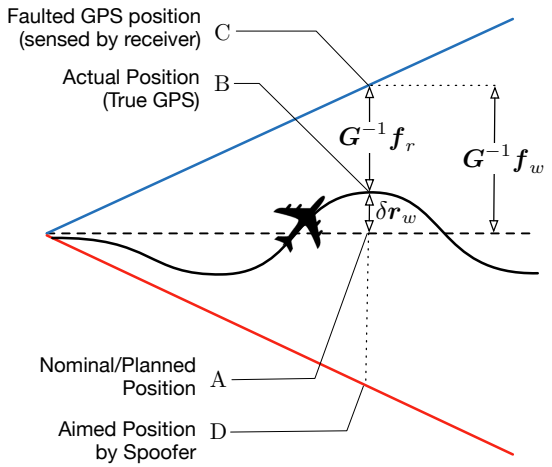

Fig. 6. Worst Case Fault and Resultant Fault Under Spoofing Attack

does not respond to the spoofed signals, thus the aircraft actual path remains at the black curve around the nominal trajectory. Knowing the nominal path of the aircraft, a smart spoofer may inject the worst-case fault leading to a hazardous situation without being detected by the aircraft monitor [5]. In the existence of wind gust – and assuming the spoofer cannot predict the actual trajectory of the aircraft – the resultant fault $\boldsymbol{f}_r$ can be expressed in terms of the worst-case fault $\boldsymbol{f}_w$ as

$$\boldsymbol{f}_r = \boldsymbol{f}_w - \boldsymbol{G}^* \, \delta\boldsymbol{r}_w \tag{37}$$

In Fig. 4, $\delta\boldsymbol{r}_w$ is defined as the deviation in position due to wind gust and it is different than the position error vector $\delta\boldsymbol{r}$ used in (28). Although we can obtain a deterministic worst-case fault vector $\boldsymbol{f}_w$ for a given nominal trajectory using [5], a spectral model for $\delta\boldsymbol{r}_w$ was derived in (21).

B. RAIM Formulation for Fault Detection Performance

Recall that using the residual based detector, it is possible to analytically determine the worst-case sequence of spoofed GPS measurements that is, the spoofed GPS signal profile that maximizes integrity risk. It should be mentioned once again that worst-case fault is computed using nominal trajectory values since it is assumed that the spoofer have knowledge of the nominal trajectory only.

Batch form of resultant fault vector $\boldsymbol{f}_{r_b}$ in (34) can be reformulated in terms of position deviation due to wind gust $\delta\boldsymbol{r}_w$ and worst-case fault $\boldsymbol{f}_w$ using (37) as

$$\boldsymbol{f}_{r_b} = \underbrace{\begin{bmatrix} 0 \\ \boldsymbol{f}_{w_1} \\ 0 \\ \boldsymbol{f}_{w_2} \\ \vdots \end{bmatrix}}_{\boldsymbol{f}_{w_b}} - \underbrace{\begin{bmatrix} 0 & & & \\ \boldsymbol{G}_1^* & & 0 & \\ & 0 & & \\ & \boldsymbol{G}_2^* & & \\ 0 & & \ddots & \end{bmatrix}}_{\boldsymbol{G}_b^*} \underbrace{\begin{bmatrix} \delta\boldsymbol{r}_{w_1}^{(n)} \\ \delta\boldsymbol{r}_{w_2}^{(n)} \\ \\ \\ \vdots \end{bmatrix}}_{\delta\boldsymbol{r}_{w_b}^{(n)}} \tag{38}$$

where $\delta \boldsymbol{r}_{w_b} \sim \mathcal{N}(0, \boldsymbol{R}_{w_b})$ and represents time history of position deviations due to wind gust. $\boldsymbol{R}_{w_b}$ is the covariance matrix of $\delta \boldsymbol{r}_{w_b}$ and can be obtained using (21). $\boldsymbol{f}_{w_b}$ is the worst-case fault profile in batch form derived in (13).

When quantifying the performance of the monitor in the existence of wind gust, we need to use the resultant fault vector $\boldsymbol{f}_{r_b}$ in the residual equation. Therefore, substituting (38) into (5) results in

$$\boldsymbol{r} = \big(\boldsymbol{I} - \boldsymbol{H}_b\, \boldsymbol{S}_b\big)\big(\boldsymbol{v}_b + \boldsymbol{f}_{w_b} - \boldsymbol{G}_b^*\, \delta \boldsymbol{r}_{w_b}\big) \tag{39}$$

The new formulation of residual in (39) captures the wind gust effect. Therefore, we can quantify the effect of the wind gust on the detection capability of RAIM in terms of integrity risk. Similarly, the state estimate error in (10) is also modified to

$$\varepsilon = \boldsymbol{s}_b^T \left(\boldsymbol{\nu}_b + \boldsymbol{f}_{w_b} - \boldsymbol{G}_b^*\, \delta \boldsymbol{r}_{w_b}\right) \tag{40}$$

In most RAIM implementations, it is proven that the test statistics and estimate errors are independent, and therefore the probability on the right hand side of (12) is written as a product of the two probabilities. However, due to the different approach we pursue to capture wind gust effect, it can be shown that the estimate error ε in (40) and test statistics q obtained from (39) are correlated. Computing the integrity risk with correlated ε and q is difficult. The norm of the parity vector was shown to be equal to the weighted norm of the actual system (test statistics) in [20]. Therefore, we can define an equivalent approach to evaluate the integrity risk by obtaining a parity vector $\boldsymbol{p}$ using the residual vector of the whitened model. The whitened actual model can be obtained as

$$\begin{aligned} \overbrace{\boldsymbol{V}_b^{-1/2}\boldsymbol{z}_b}^{\overline{\boldsymbol{z}}_b} = \overbrace{\boldsymbol{V}_b^{-1/2}\boldsymbol{H}_b}^{\overline{\boldsymbol{H}}_b}\, \boldsymbol{x}_b + \overbrace{\boldsymbol{V}_b^{-1/2}\boldsymbol{\nu}_b}^{\overline{\boldsymbol{\nu}}_b} + \overbrace{\boldsymbol{V}_b^{-1/2}\boldsymbol{f}_{w_b}}^{\overline{\boldsymbol{f}}_{w_b}} \\ - \underbrace{\boldsymbol{V}_b^{-1/2}\boldsymbol{G}_b^*}_{\overline{\boldsymbol{G}}_b^*}\, \delta \boldsymbol{r}_{w_b} \end{aligned} \tag{41}$$

where $\overline{\boldsymbol{\nu}}_b \sim \mathcal{N}\big(\boldsymbol{0}, \boldsymbol{I}\big)$. Note that the bars represents the whitened actual system. Residual vector of the whitened system becomes

$$\overline{\boldsymbol{r}} = \big(\boldsymbol{I} - \overline{\boldsymbol{H}}_b - \overline{\boldsymbol{S}}_b\big)\big(\overline{\boldsymbol{v}}_b + \overline{\boldsymbol{f}}_{w_b} - \overline{\boldsymbol{G}}_b^*\, \delta \boldsymbol{r}_{w_b}\big) \tag{42}$$

it is defined as

$$\boldsymbol{p} = \boldsymbol{L}\, \overline{\boldsymbol{r}} \tag{43}$$

where $\boldsymbol{L}$ is the unitary left null-space matrix of $\overline{\boldsymbol{H}}_b$ such that $\boldsymbol{L}\overline{\boldsymbol{H}}_b = 0$ and can be obtained using singular value decomposition of $\overline{\boldsymbol{H}}_b$ as

$$\overline{\boldsymbol{H}}_b = [\boldsymbol{U}_1 \;\; \boldsymbol{U}_2] \begin{bmatrix} \boldsymbol{S} \\ 0 \end{bmatrix} \boldsymbol{V}^T \tag{44}$$

$$\boldsymbol{L} = \boldsymbol{U}_2^T \tag{45}$$

The parity vector $\boldsymbol{p}$ in (43) can be expanded as

$$\boldsymbol{p} = \boldsymbol{L}\big(\overline{\boldsymbol{v}}_b + \overline{\boldsymbol{f}}_{w_b} - \overline{\boldsymbol{G}}_b^*\, \delta \boldsymbol{r}_{w_b}\big) \tag{46}$$

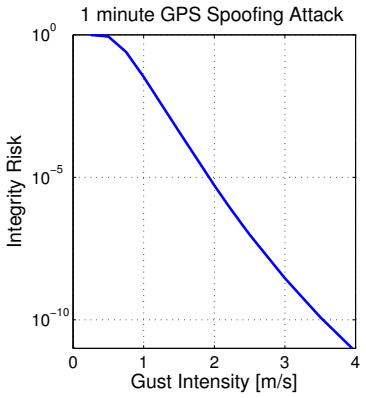

Fig. 7. The impact of wind gust intensity on integrity risk after 60 seconds level flight of Boeing 747 aircraft under worst-case GPS spoofing attack

where $\boldsymbol{p}$ is composed of $(n - m)$ independent Gaussian distributions, where n and m are the number of measurement and states in the batch, respectively.

Combining the parity vector in (46) and the state estimate error in (40), we obtain a multi-dimensional Gaussian distribution as

$$[\boldsymbol{p}, \varepsilon]^T \sim \mathcal{N}\big(\boldsymbol{\mu}, \boldsymbol{\Sigma}\big) \tag{47}$$

where the mean vector $\boldsymbol{\mu}$ is

$$\boldsymbol{\mu} = \begin{bmatrix} \boldsymbol{L} \\ \overline{\boldsymbol{s}}_b^T \end{bmatrix} \overline{\boldsymbol{f}}_{w_b} \tag{48}$$

and covariance matrix $\boldsymbol{\Sigma}$ is

$$\boldsymbol{\Sigma} = \begin{bmatrix} \mathbb{E}\{\boldsymbol{p}\boldsymbol{p}^T\} & \mathbb{E}\{\varepsilon \boldsymbol{p}^T\} \\ \mathbb{E}\{\boldsymbol{p}\varepsilon^T\} & \mathbb{E}\{\varepsilon\varepsilon^T\} \end{bmatrix} \tag{49}$$

where

$$\mathbb{E}\{\boldsymbol{p}\boldsymbol{p}^T\} = \boldsymbol{I} + \boldsymbol{L}\, \overline{\boldsymbol{G}}_b^*\, \boldsymbol{R}_{w_b}\, \overline{\boldsymbol{G}}_b^{*^T}\, \boldsymbol{L}^T \tag{50}$$

$$\mathbb{E}\{\varepsilon\varepsilon^T\} = \overline{\boldsymbol{s}}_b^T \big(\overline{\boldsymbol{G}}_b^*\, \boldsymbol{R}_{w_b}\, \overline{\boldsymbol{G}}_b^{*^T} + \boldsymbol{I}\big)\, \overline{\boldsymbol{s}}_b \tag{51}$$

$$\mathbb{E}\{\varepsilon \boldsymbol{p}^T\} = \overline{\boldsymbol{s}}_b^T\, \overline{\boldsymbol{G}}_b^*\, \boldsymbol{R}_{w_b}\, \overline{\boldsymbol{G}}_b^{*^T}\, \boldsymbol{L}^T \tag{52}$$

The correlated terms in the covariance matrix in (49) are due to the dependency between $\boldsymbol{p}$ and ε. The integrity risk for a given gust power spectral density and spoofing hypothesis H_s in (53), can be solved numerically using the multi-dimensional Gaussian distribution derived in (47).

$$I_r = P\{|\varepsilon| > l,\, |\boldsymbol{p}_i| < T \,|H_s\} \tag{53}$$

where $i = 1, .., (n-m)$. l is defined as the vertical alert limit, and T is the same threshold for the actual detector defined in (12).

VI. SIMULATION RESULTS

In this section, a covariance analysis is implemented to quantify the impact of wind gust on the integrity risk during precision approach landing under worst case GPS spoofing scenario. we assumed that a spoofer has a limited range, therefore the spoofing attack is of short duration. Boeing 747

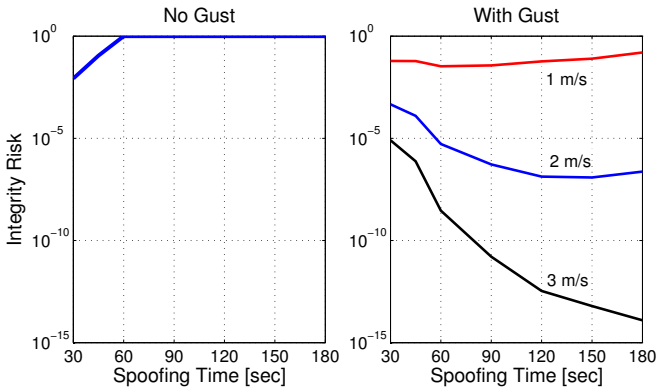

Fig. 8. The impact of GPS Spoofing Attack Duration on Integrity Risk for Boeing 747 flight in gust-free case and in the existence of wind gust intensities σ_g ranging from 1 to 3 m/s

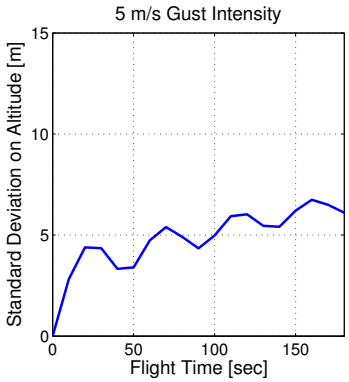

Fig. 9. The effect of 5 m/s gust power spectral density on state estimate covariances of altitude for 3 minute Boeing 747 commercial aircraft flight

TABLE I
STEADY-STATE STANDARD DEVIATIONS IN VERTICAL DYNAMICS OF BOEING 747 COMMERCIAL AIRCRAFT EXPOSED TO 5 M/S GUST INTENSITY

Standard Deviation	Symbol	Value	Unit
Heading Speed	σ_u	1.42	m/s
Vertical Speed	σ_w	0.24	m/s
Pitch Angle Rate	σ_q	0.13	deg/s
Pitch Angle	σ_θ	0.37	deg

commercial aircraft model is selected to test the performance of the RAIM Monitor with a spoofing attack under various vertical wind gust conditions. The aircraft properties are given in Table III in Appendix E.

The aircraft is assumed to descend in trimmed (level) flight conditions and only the vertical aircraft and gust dynamics are investigated. The nominal flight conditions and corresponding longitudinal aerodynamic coefficients with their derivatives for trimmed flight conditions are given in Table IV and V in Appendix E.

In this analysis, we assume that the aircraft is running a Kalman filter for at least 10 seconds prior to starting the monitor and the GPS spoofing attack. The INS and GPS receiver specifications can be found in Table V in Appendix E.

In Fig. 7, the results illustrate that integrity risk considerably diminishes as the wind gust intensity (power spectral density) increases for a worst-case spoofing attack lasting up to 1 minute. The results showed that even for light turbulence condition ($\sigma_g < 2.5$ m/s) [10], integrity risk in the order of (10^{-7}) can be achieved. This is a promising result since, although we conservatively select one of the biggest aircraft which may be least impacted by wind gusts, the minimum wind gust intensity required for detecting worst-case spoofing scenario is low.

To investigate the impact of spoofing time over integrity risk, we ran simulations in which wind gust intensity changes from 0 to 3 m/s and spoofing attack periods of 30 sec to 3 min.

The left hand side plot in Fig. 8 shows the case with no wind gust under worst case spoofing. The spoofing integrity risk sharply increases to approximately 1 as time increases from 30 sec to 1 min. We conclude that under no-gust condition, increasing the spoofing time allows the spoofer to inject faults to the system more slowly, which reduces the detectability of RAIM while corrupting INS and increasing the integrity risk. On the other hand, with very light wind gust intensities ($\sigma_g < 1$ m/s), it is observed in the right hand plot of Fig. 8 that although the spoofer achieves to tease off the aircraft slightly over time, the integrity risk is still better than gust-free case. Furthermore, Fig. 8 shows that with sufficient wind gust intensity ($\sigma_g > 2$ m/s), increasing spoofing time allows much better detection of GPS spoofing since the discrepancy between the actual position due to wind gust and the nominal position assumed by the spoofer grows more over time. As a result, the integrity risk decreases over time unlike gust-free case. This clearly proves that wind gust enhances the detection capability of INS-RAIM system as the spoofing time elapses.

To illustrate that the wind gust intensity values used to generate Fig. 8 are realistic, we simulate 3 minute flight of Boeing 747 exposed to an exaggerated value of 5 m/s gust intensity. The steady-state standard deviations in vertical dynamics of the aircraft are given in Table I. For example, the steady-state standard deviation in vertical speed of the aircraft is about 0.25 m/s in the existence of 5 m/s wind gust intensity. Using these steady-state values, the growth in altitude error is in Fig. 9. The standard deviation in vertical position reaches approximately 6 m in 3 min. These values are seem realistic given the size of the aircraft and and landing approach. Therefore, it can be concluded that, although the wind gust values we used are not aggressive, it enhances the detection capability against a worst-case spoofing attack while achieving very small integrity risk values. Recall that these simulations assume that the spoofer has no knowledge of the actual aircraft trajectory during the approach. The impact of this assumption on INS-RAIM performance will be investigated in the future.

VII. CONCLUSION

In this work, we investigated wind gust impact on detection capability of aircraft against worst-case GPS spoofing attacks. Unlike conventional methods using deterministic wind gust

profiles, we developed a generalized statistical approach to quantify the enhancement in detection of GPS spoofing attacks for given stochastic information about vertical wind gust. The derived methodology enables us to predict integrity risk under GPS spoofing attack with a worst-case fault for a given planned (nominal) trajectory. To quantify the detector performance, we performed a covariance analysis using a tightly-coupled INS-GPS in batch form and a power spectral wind turbulence model to obtain aircraft's response to wind gusts. We also defined a novel formulation for RAIM with INS coupling, where the impact of wind gust disturbances on the integrity risk against spoofing attacks can be quantified numerically. The covariance analyses we conducted, prove that, for INS-RAIM-equipped aircraft, the aircraft response to wind gust provides a direct means for detection of GPS spoofing even if a worst-case fault profile is injected by the spoofer.

ACKNOWLEDGMENT

The authors gratefully acknowledge the FAA for supporting this research. However, the opinions presented in this paper are those of the authors alone and do not necessarily represent those of the FAA or any other affiliated agencies.

Appendix A
THE DRYDEN GUST MODEL

This appendix explains the Dryden's continuous power spectral model for the vertical wind gust. It defines vertical translational velocity with a second order transfer function G_{w_g} parameterized by standard deviation on gust intensity σ_g, turbulence length L_w and velocity of the aircraft $\boldsymbol{v}$ as [10]

$$G_{w_g}(s) = \sigma_g \frac{\sqrt{\frac{|\boldsymbol{v}|^3}{\pi {L_w}^3}} + \sqrt{\frac{3|\boldsymbol{v}|}{\pi L_w}}s}{\frac{|\boldsymbol{v}|^2}{L_w^2} + \frac{2|\boldsymbol{v}|}{L_w}s + s^2} \tag{54}$$

It also relates the vertical velocity and pitch rate of the gust with a first order transfer function parameterized by the wingspan of the aircraft b as [10]

$$G_{q_g}(s) = \frac{\frac{s}{|\boldsymbol{v}|}}{1 + \left(\frac{4b}{\pi|\boldsymbol{v}|}\right)s} \tag{55}$$

The combined third-order gust dynamics model can be represented with 3 states in controllable-canonical state-space form as

$$\begin{bmatrix} \dot{x}_{w_1} \\ \dot{x}_{w_2} \\ \dot{x}_q \end{bmatrix} = \overbrace{\begin{bmatrix} 0 & 1 & 0 \\ -\frac{|\boldsymbol{v}|^2}{L_w^2} & -\frac{2|\boldsymbol{v}|}{L_w} & 0 \\ \frac{\pi\sigma_g}{4b}\sqrt{\frac{|\boldsymbol{v}|^3}{\pi L_w^3}} & \frac{\pi\sigma_g}{4b}\sqrt{\frac{3|\boldsymbol{v}|}{\pi L_w}} & -\frac{4b}{\pi|\boldsymbol{v}|} \end{bmatrix}}^{\boldsymbol{A}_g} \overbrace{\begin{bmatrix} x_{w_1} \\ x_{w_2} \\ x_q \end{bmatrix}}^{\boldsymbol{x}_g} + \underbrace{\begin{bmatrix} 0 \\ 1 \\ 0 \end{bmatrix}}_{\boldsymbol{b}_g} \eta_g \tag{56}$$

where $\eta_g \sim \mathcal{N}(0, \sigma_g^2)$. The first two elements in $\boldsymbol{x}_g$ are vertical gust states, and the last element is related to pitch rate. The disturbances to wind vertical velocity and longitudinal angular velocity can be output as a function of gust states as

$$\underbrace{\begin{bmatrix} w_q \\ q_g \end{bmatrix}}_{\boldsymbol{w}_g} = \underbrace{\begin{bmatrix} 0 & \frac{\pi\sigma_g}{4b}\sqrt{\frac{|\boldsymbol{v}|^3}{\pi L_w^3}} & \frac{\pi\sigma_g}{4b}\sqrt{\frac{3|\boldsymbol{v}|}{\pi L_w}} \\ 0 & 0 & \frac{1}{|\boldsymbol{v}|} \end{bmatrix}}_{\boldsymbol{c}_g^T} \boldsymbol{x}_g \tag{57}$$

Driving the linear and angular filters G_{w_g} and G_{q_g} with independent, unit variance white noise η_g yields linear vertical gust velocity w and angular pitch rate q.

Appendix B
AIRCRAFT FLIGHT DYNAMIC MODEL

This appendix is for the derivation of linearized vertical aircraft dynamics. Nonlinear aircraft longitudinal equations of motion in the form of coupled state equations are given as [12]

$$I_{22}\dot{q} + (I_{33} - I_{11})pr + I_{13}(r^2 - p^2) = M_2^a \tag{58}$$

$$m(\dot{u} + qw - rv) = -mgsin\theta + T - Dcos\beta cos\alpha + Lsin\alpha \tag{59}$$

$$m(\dot{w} + pv - qu) = mgcos\theta cos\phi - Dcos\beta sin\alpha + Lcos\alpha \tag{60}$$

where u, v, w are the velocity components in body axes in Fig. 16, p, q, r are roll, pitch, and yaw rates, α, β, θ are angle of attack, side slip angle and flight path angle, m is the aircraft mass; I_{11}, I_{22}, I_{33} are mass moment of inertias represented in body frame; T, D, L, M_2^a are thrust and aero forces including drag, lift, pitch moment. The three longitudinal EOMs in (19), (22) and (**??**) consist of the x-force, z-force, and y-moment equations.

As we assume a perturbed flight due to wind gust around a nominal trajectory, the nonlinear equations of motions (EOM) can be linearized by recasting each variable in terms of perturbed variables and corresponding nominal values, which are the trimmed flight conditions ($p = q = r = 0$). In order to uncouple lateral and longitudinal dynamics in (19), we also assumed a straight and symmetric flight ($\phi = \beta = 0$) in

the vertical plane ($v = 0$). These simplifications produce a perturbed inertial forces and moment as [12]

$$\delta F_1^i = m(\delta\dot{u} + w^*\delta q) \tag{61}$$

$$\delta F_3^i = m(\delta\dot{w} - u^*\delta q) \tag{62}$$

$$\delta M_2^i = I_{22}\,\delta\dot{q} \tag{63}$$

where superscript $(^*)$ represents the nominal values, which are constant. Also, external forces and moments can be simplified by assuming a constant thrust as [12]

$$\delta D = D_u\delta u + D_\alpha\delta\alpha + D_{\dot{\alpha}}\delta\dot{\alpha} + D_q\delta q + D_{\delta_e}\delta(\delta_e) \tag{64}$$

$$\delta L = L_u\delta u + L_\alpha\delta\alpha + L_{\dot{\alpha}}\delta\dot{\alpha} + L_q\delta q + L_{\delta_e}\delta(\delta_e) \tag{65}$$

$$\delta M_2^a = M_u\delta u + M_\alpha\delta\alpha + M_{\dot{\alpha}}\delta\dot{\alpha} + M_q\delta q + M_{\delta_e}\delta(\delta_e) \tag{66}$$

where symbols with subscripts indicate aerodynamic coefficients and their derivatives with respect to speed, angle of attack, pitch rate and control deflection. Under small variations in angle of attack around zero, angle of attack can be expressed in terms of vertical body speed and total speed of the aircraft as

$$\delta\alpha = \frac{\delta w}{|\boldsymbol{v}|} \tag{67}$$

Assuming that control surfaces are fixed ($\delta = 0$) and equating inertial forces and moment in (61) to (63) to the external forces and moment in (64) to (66) respectively, yields a state space form of EOM describing longitudinal aircraft dynamics as

$$\begin{bmatrix}\delta\dot{u}\\ \delta\dot{w}\\ \delta\dot{q}\\ \delta\dot{\theta}\end{bmatrix} = \underbrace{\begin{bmatrix} -\frac{D_u}{m} & \frac{L^*-D_\alpha}{m|\boldsymbol{v}|} & \frac{-D_q}{m}-w^* & -gc\theta^*\\ \frac{L_u}{m} & \frac{L_\alpha-D^*}{m|\boldsymbol{v}|} & \frac{L_q}{m}+u^* & -gs\theta^*\\ \frac{M_u}{I_{22}} & \frac{M_\alpha}{I_{22}|\boldsymbol{v}|} & \frac{M_q}{I_{22}} & 0\\ 0 & 0 & 1 & 0\end{bmatrix}}_{\boldsymbol{F}_d} \underbrace{\begin{bmatrix}\delta u\\ \delta w\\ \delta q\\ \delta\theta\end{bmatrix}}_{\delta\boldsymbol{x}_d} \tag{68}$$

where the plant matrix $\boldsymbol{F}_d$ is a constant matrix that includes terms related to trimmed flight aerodynamic coefficients, mass and inertial properties of the aircraft. It has short and long period (phugoid) modes.

Appendix C
INS ERROR KINEMATICS MODEL

This appendix includes the derivations for the INS mechanization equations. Before starting linearization, the significant assumptions are listed as

1) Navigation frame N is fixed at the ground reference station r (Fig. 3).
2) Position $\boldsymbol{r}$ and attitude $\boldsymbol{E}$ of the aircraft in mechanization equations are with respect to position of the reference station.
3) Velocity of the aircraft $\boldsymbol{v}$ is not the inertial velocity but the ground velocity.
4) Since we assume a level flight, all of the nominal values of variations are assumed to be constant in linearization.
5) Gravity vector error variations are not modeled in the velocity error equation since their contribution over the duration of an aircraft approach is negligibly small.

Using the assumptions above, nonlinear kinematic equations of the aircraft [13] can be obtained as

$$\dot{\boldsymbol{x}}_n \triangleq \begin{bmatrix}\dot{\boldsymbol{r}}^{(n)}\\ \dot{\boldsymbol{v}}^{(n)}\\ \dot{\boldsymbol{E}}^{(n)}\end{bmatrix} = \begin{bmatrix}\boldsymbol{v}^{(n)}\\ {}^N\boldsymbol{R}^B\boldsymbol{f}^{(b)} - 2\tilde{\boldsymbol{\omega}}_{ie}^{(n)}\boldsymbol{v}^{(n)} + \boldsymbol{g}^{(n)}\\ \boldsymbol{Q}_{BE}^{-1}\{\boldsymbol{\omega}_{ib}^{(b)} - {}^N\boldsymbol{R}^E\boldsymbol{\omega}_{ie}^{(e)}\}\end{bmatrix} \tag{69}$$

where the INS state vector $\boldsymbol{x}_n$ is defined in N-frame and composed of position relative to reference station $\boldsymbol{r}^{(n)}$, ground velocity $\boldsymbol{r}^{(n)}$, and attitude (Euler angles) $\boldsymbol{E}^{(n)}$. Also, ${}^N\boldsymbol{R}^B$ and ${}^N\boldsymbol{R}^E$ are rotation matrices from body and earth to navigation frame respectively; $\boldsymbol{Q}_{BE}$ is the matrix that transforms Euler angle rates to body rotation rates, and $\tilde{\boldsymbol{\omega}}_{ie}$ and $\tilde{\boldsymbol{\omega}}_{ib}$ are the skew symmetric matrices of angular velocity vectors of earth and body with respect to I-frame. Also, $\boldsymbol{f}_b$ is the specific force acting on aircraft. Note that the superscripts with parentheses refer to the frame in which the vector is expressed.

Expressing all the variables in (69) in perturbation form in [13], position and velocity error equations come out as

$$\delta\dot{\boldsymbol{r}}^{(n)} = \delta\boldsymbol{v}^{(n)} \tag{70}$$

$$\delta\dot{\boldsymbol{v}}^{(n)} = \left[{}^N\boldsymbol{R}^{B^*}\tilde{\boldsymbol{f}}^{(b)^*}\right]\delta\boldsymbol{E} + \left[{}^N\boldsymbol{R}^{B^*}\right]\delta\boldsymbol{f}^{(b)} + \left[-2\,\tilde{\boldsymbol{\omega}}_{ie}^{(n)}\right]\delta\boldsymbol{v}^{(n)} \tag{71}$$

where $\tilde{\boldsymbol{f}}^{(b)^*}$ is the skew symmetric matrix of specific force acting on aircraft flying over nominal trajectory, and ${}^N\boldsymbol{R}^{B^*}$ is rotation matrix for the nominal B-frame to N-frame. Variation on gravity vector is not modeled in the velocity error equation since its contribution over the duration of an aircraft approach is negligibly small.

Using the summation rule for angular velocities, we can write attitude rate $\dot{\boldsymbol{E}}^{(n)}$ as a function of body angular rate $\boldsymbol{\omega}_{ib}^{(b)}$ and Earth's constant rotation rate $\boldsymbol{\omega}_{ie}^{(e)}$ relative to inertial frame as

$$\dot{\boldsymbol{E}}^{(n)} = \boldsymbol{Q}_{BE}^{-1}\underbrace{\left[\boldsymbol{\omega}_{ib}^{(b)} - {}^B\boldsymbol{R}^N\boldsymbol{\omega}_{ie}^{(n)}\right]}_{\boldsymbol{s}} \tag{72}$$

Using the definition of $\boldsymbol{s}$ in (72), we can apply Taylor Series Expansion to linearize the attitude equation as

$$\delta\dot{\boldsymbol{E}}^{(n)} = \boldsymbol{Q}_{BE}^{*-1}\,\delta\boldsymbol{\omega}_{ib}^{(b)} + \overbrace{\begin{bmatrix}\boldsymbol{s}^{*^T} & 0 & 0\\ 0 & \boldsymbol{s}^{*^T} & 0\\ 0 & 0 & \boldsymbol{s}^{*^T}\end{bmatrix}}^{\boldsymbol{S}^*}\delta\boldsymbol{Q}_{BE}^{-1} + \underbrace{\begin{bmatrix}\boldsymbol{\omega}_{ie}^{(n)^T} & 0 & 0\\ 0 & \boldsymbol{\omega}_{ie}^{(n)^T} & 0\\ 0 & 0 & \boldsymbol{\omega}_{ie}^{(n)^T}\end{bmatrix}}_{\boldsymbol{W}_{ie}}\delta^B\boldsymbol{R}^N \tag{73}$$

where $\delta \boldsymbol{Q}_{BE}^{-1}$ and $\delta^B \boldsymbol{R}^N$ can be written in terms of $\delta \boldsymbol{E}^{(n)}$ as

$$\delta \boldsymbol{Q}_{BE}^{-1} = \left. \frac{\partial \boldsymbol{Q}_{BE}^{-1}}{\partial \boldsymbol{E}^{(n)}} \right|_* \delta \boldsymbol{E}^{(n)} \tag{74}$$

$$\delta^B \boldsymbol{R}^N = \left. \frac{\partial^B \boldsymbol{R}^N}{\partial \boldsymbol{E}^{(n)}} \right|_* \delta \boldsymbol{E}^{(n)} \tag{75}$$

Let us define a matrix called $\boldsymbol{K}^*$ containing only constant nominal parameters as

$$\boldsymbol{K}^* = \boldsymbol{S}^* \left. \frac{\partial \boldsymbol{Q}_{BE}^{-1}}{\partial \boldsymbol{E}^{(n)}} \right|_* + \boldsymbol{W}_{ie} \left. \frac{\partial^B \boldsymbol{R}^N}{\partial \boldsymbol{E}^{(n)}} \right|_* \tag{76}$$

and substituting Equations (74) to (76) into (73) yields attitude error equation as

$$\delta \dot{\boldsymbol{E}}^{(n)} = \boldsymbol{Q}_{BE}^{*-1} \delta \boldsymbol{\omega}_{ib}^{(b)} + \boldsymbol{K}^* \delta \boldsymbol{E}^{(n)} \tag{77}$$

The overall linearized INS kinematic model can be expressed in vector form as

$$\begin{bmatrix} \delta \dot{\boldsymbol{r}}^{(n)} \\ \delta \dot{\boldsymbol{v}}^{(n)} \\ \delta \dot{\boldsymbol{E}}^{(n)} \end{bmatrix} = \overbrace{\begin{bmatrix} 0 & 1 & 0 \\ 0 & -2\,\tilde{\boldsymbol{\omega}}_{ie}^{(n)} & {}^N\boldsymbol{R}^{B^*}\tilde{\boldsymbol{f}}^{(b)^*} \\ 0 & 0 & \boldsymbol{K}^* \end{bmatrix}}^{\boldsymbol{F}_n} \overbrace{\begin{bmatrix} \delta\, \boldsymbol{r}^{(n)} \\ \delta\, \boldsymbol{v}^{(n)} \\ \delta\, \boldsymbol{E}^{(n)} \end{bmatrix}}^{\delta \boldsymbol{x}_n} + \underbrace{\begin{bmatrix} 0 & 0 \\ {}^N\boldsymbol{R}^{B^*} & 0 \\ 0 & \boldsymbol{Q}_{BE}^{*-1} \end{bmatrix}}_{\boldsymbol{G}_u} \underbrace{\begin{bmatrix} \delta \boldsymbol{f}^{(b)} \\ \delta \boldsymbol{\omega}_{ib}^{(b)} \end{bmatrix}}_{\delta \boldsymbol{u}} \tag{78}$$

where $\delta \boldsymbol{x}_n$ is referred to as the INS state vector, $\boldsymbol{F}_n$ is plant matrix of the kinematic model, $\boldsymbol{G}_u$ is input coefficient matrix, and $\delta \boldsymbol{u}$ is the variation on IMU measurements, which are the specific force and angular velocity of the aircraft. Note that all the superscripts $*$ refers to constant nominal values.

Appendix D
GPS MEASUREMENT MODEL

This appendix gives a linearized measurement model for DD carrier and code GPS [15] in the form of

$$\underbrace{\begin{bmatrix} \boldsymbol{\phi} \\ \hline \boldsymbol{\rho} \end{bmatrix}}_{\boldsymbol{z}} = \underbrace{\begin{bmatrix} \boldsymbol{G}' \\ \hline \boldsymbol{G}' \end{bmatrix}}_{\boldsymbol{G}^*} \delta \boldsymbol{r}^{(e)} + \underbrace{\begin{bmatrix} \lambda \boldsymbol{I} \\ \hline 0 \end{bmatrix}}_{\boldsymbol{D}} \boldsymbol{N} + \underbrace{\begin{bmatrix} \boldsymbol{\nu}_\phi \\ \hline \boldsymbol{\nu}_\rho \end{bmatrix}}_{\boldsymbol{\nu}_{\rho\phi}} \tag{79}$$

where λ is L1 carrier frequency, N is cycle ambiguity states, $\boldsymbol{r}^{(e)}$ is position from reference station expressed in E-frame. ϕ and ρ are carrier and code measurements after correcting for the nominal term $\boldsymbol{G}^* \delta \boldsymbol{r}^*$. $\boldsymbol{G}'$ is observation matrix including line-of-sight vectors from reference station to n-satellites as

$$\boldsymbol{G}' = \begin{bmatrix} -\left(\boldsymbol{e}_2^T - \boldsymbol{e}_1^T\right) \\ \vdots \\ -\left(\boldsymbol{e}_n^T - \boldsymbol{e}_1^T\right) \end{bmatrix} \tag{80}$$

where $\boldsymbol{e}_i$ represents the unit line-of-sight vector of the i^{th} satellite in E-frame. The DD carrier and code phase measurement errors $\boldsymbol{\nu}_\phi$ and $\boldsymbol{\nu}_\rho$, are assumed to be zero-mean Gaussian distribution with a covariance which can be expressed in terms of single difference (SD) code and carrier measurement standard deviations σ_ϕ and σ_ρ as

$$\begin{aligned} \boldsymbol{\nu}_\phi &\sim \mathcal{N}(0, \boldsymbol{\Lambda}\boldsymbol{\Lambda}^T \sigma_\phi^2) \\ \boldsymbol{\nu}_\rho &\sim \mathcal{N}(0, \boldsymbol{\Lambda}\boldsymbol{\Lambda}^T \sigma_\rho^2) \end{aligned} \tag{81}$$

where $\boldsymbol{\Lambda}$ is the transformation matrix that transforms SD measurement noise vector to DD noise vector. Note that DD method allows eliminating ephemeris, satellite and receiver clock errors for improving the accuracy in descending phase of the flight.

Appendix E
SIMULATION DATA

TABLE II
INS-GPS ERROR PARAMETERS [18]

Parameter	Value	Unit
Gyro angle random walk	0.001	$^o/\sqrt{h}$
Gyro bias error	0.01	$^o/h$
Gyro time constant	3600	s
Accelerometer white noise	$10^{-5}g$	m/s^2
Accelerometer bias error	$10^{-5}g$	m/s^2
Accelerometer bias time constant	3600	s
Multipath time constant	100	s
SD Carrier phase multipath noise	1	cm
SD Code phase multipath noise	30	cm
SD Carrier phase thermal noise	0.2	cm
SD Code phase thermal noise	50	cm

TABLE III
BOEING 747 AIRCRAFT PROPERTIES [19]

Properties	Symbol	Value	Unit
Mass	m	$289,550$	kg
Moment of Inertia	I_{yy}	44.87×10^6	$kg.m^2$
Wing Span	b	59.74	m
Wing Chord	c	8.32	m
Wing Area	S	510.96	m^2

TABLE IV
AERODYNAMIC COEFFICIENTS AND DERIVATIVES [19]

	Drag	Lift	Pitch
Coefficient	0.266	-0.0174	0
AoA Derivative	0.084	4.24	-0.629
Speed Derivative	-0.0064	-0.084	-0.0928
Pitch Rate Derivative	0	-0.0928	-20.5

TABLE V
VERTICAL FLIGHT CONDITIONS [19]

Flight Conditions	Symbol	Value	Unit
Aircraft Speed	$\|\boldsymbol{v}\|$	85	m/s
Turbulence Scale Length	L_w	1750	$kg.m^2$
Angle of Attack	α	0	m
Flight Path Angle	θ	-5	deg
Air Density	ρ_a	11.853	kg/m^3
Altitude	h	500	m

References

[1] Humphreys, T. E., Ledvina, B. M., Psiaki, M. L., O'Hanlon, B. W., Kintner, P. M. Jr., "Assessing the Spoofing Threat: Development of a Portable GPS Civilian Spoofer," Proceedings of the 21st International Technical Meeting of the Satellite Division of The Institute of Navigation (ION GNSS 2008), Savannah, GA, September 2008, pp. 2314-2325.

[2] Wesson, K. D., Rothlisberger, M. P., Humphreys, T. E., "A Proposed Navigation Message Authentication Implementation for Civil GPS Anti-Spoofing," Proceedings of the 24th International Technical Meeting of The Satellite Division of the Institute of Navigation (ION GNSS 2011), Portland, OR, September 2011, pp. 3129-3140.

[3] Akos, Dennis M., "Whos Afraid of the Spoofer? GPS/GNSS Spoofing Detection via Automatic Gain Control (AGC)", NAVIGATION, Journal of The Institute of Navigation, Vol. 59, No. 4, Winter 2012, pp. 281-290.

[4] Mark L. Psiaki, Steven P. Powell, and Brady W. OHanlon, GNSS Spoofing Detection Using High-Frequency Antenna Motion and Carrier-Phase Data, Proceedings of the 26th International Technical Meeting of The Satellite Division of the Institute of Navigation (ION GNSS 2013), Nashville, TN, September 2013

[5] Joerger, M., F.-C. Chan, S. Langel, and B. Pervan. RAIM Detector and Estimator Design to Minimize the Integrity Risk. Proceedings of the 25th International Technical Meeting of The Satellite Division of the Institute of Navigation (ION GNSS 2012). Nashville, TN. (2012).

[6] Khanafseh, S., Roshan, N., Langel, S. , Chan, F., Joerger, M., Pervan, B. GPS Spoofing Detection Using RAIM with INS Coupling, Position, Location and Navigation Symposium - PLANS 2014, 2014 IEEE/ION

[7] Warner, J. S., Johnston, R. G. (2003). GPS Spoofing Countermeasures. Homeland Security Journal.

[8] Rustenburg, J. W., Skinn, D., Tipps, D. O. (1999). An evaluation of methods to separate maneuver and gust load factors from measured acceleration time histories (No. URD-TM-1998-00011). Dayton University OH, Structural Integrity Division.

[9] Dogan, A., Lewis, T. A., Blake, W. (2008). Flight data analysis and simulation of wind effects during aerial refueling. Journal of Aircraft, 45(6), 2036-2048.

[10] Moorhouse, D. J., Woodcock, R. J. (1982). Background information and user guide for MIL-F-8785C, military specification-flying qualities of piloted airplanes (No. AFWAL-TR-81-3109). Air Force Wright Aeronautical Labs Wright-Patterson AFB OH.

[11] Cook, M. V. (2012). Flight dynamics principles: a linear systems approach to aircraft stability and control. Butterworth-Heinemann.

[12] Morris, S., L., Bossert, D., E., Hallgren, W., F., Introduction to Aircraft Flight Mechanics, AIAA Education Series. ISBN-13: 978-1624102547

[13] Farrell, J. (2008). Aided navigation: GPS with high rate sensors. McGraw-Hill, Inc.

[14] Crassidis, J. L., Junkins, J. L. (2011). Optimal estimation of dynamic systems. CRC press.

[15] Misra, P., Enge, P. (2006). Global Positioning System: Signals, Measurements and Performance Second Edition. Lincoln, MA: Ganga-Jamuna Press.

[16] Joerger, M., B. Pervan, Kalman Filter-Based Integrity Monitoring Against Sensor Faults, Journal of Guidance, Control, and Dynamics, Vol. 36, No. 2 (2013), pp. 349-361.

[17] Hoblit, F. M. (1988). Gust Loads on Aircraft: Concepts and Applications. AIAA.

[18] Brown, R. G., P. Y. C Hwang, Introduction to Random Signals and Applied Kalman Filtering. 3rd Ed. New York: John Wiley Sons, 1997.

[19] Heffley, R. K., Jewell, W. F. (1972). Aircraft Handling Qualities Data.

[20] Pervan, Boris S., David G. Lawrence, and Bradford W. Parkinson. "Autonomous fault detection and removal using GPS carrier phase." Aerospace and Electronic Systems, IEEE Transactions on 34.3 (1998): 897-906.

[21] Angus, J. E., RAIM with Multiple Faults, NAVIGATION, Vol. 53, No. 4, Winter 2006-2007, pp. 249-257.